

# Performance Evaluation of the Symmetrical Quasi-Classical Dynamics Method based on Meyer-Miller-Stock-Thoss Mapping Hamiltonian in the Treatment of Extensive Spin-Boson Models

*Yu Xie<sup>a</sup>, Jie Zheng<sup>b</sup> and Zhenggang Lan<sup>\*a</sup>*

<sup>a</sup> Key Laboratory of Biobased Materials, Qingdao Institute of Bioenergy and Bioprocess Technology, Chinese Academy of Sciences, Qingdao, 266101 Shandong, China

<sup>b</sup> Industrial Research Institute of Nonwovens & Technical Textiles, College of Textiles & Clothing, Qingdao University, Qingdao 266071, China

## **Abstract**

The symmetrical quasi-classical dynamics method based on the Meyer-Miller-Stock-Thoss mapping Hamiltonian (MMST-SQC) shows great potential in the treatment of the nonadiabatic dynamics of complex systems. We performed the comprehensive benchmark calculations to evaluate the performance of the MMST-SQC method in various spin-boson models with respect to the accurate quantum dynamics method multilayer multiconfigurational time-dependent Hartree (ML-MCTDH). The parameters of the spin-boson models are chosen to represent a few of prototypes used in the description of photoinduced charge/energy transfer

processes in photoharvesting systems and organic solar cells, which include the rather board situations with the fast or slow bath and different system-bath couplings. When the characteristic frequency of the bath is low, the MMST-SQC method performs extremely well, and it gives almost the identical results to those of ML-MCTDH in the weak system-bath coupling cases. When the fast bath is considered, however, the deviations exist between the MMST-SQC and ML-MCTDH methods, and such deviations become more significant with the larger system-bath coupling. The possible dependence of the MMST-SQC dynamics on the different initial samplings of the nuclear degrees of freedom is also discussed.

## **1. INTRODUCTION**

The theoretical understanding of nonadiabatic processes is a very challenging topic because the Born–Oppenheimer approximation breaks down due to the involvement of strongly coupled nuclear/electronic motions.<sup>1-3</sup> In last decades considerable efforts were made to develop various theoretical methods, from full quantum dynamics to different versions of semi-classical or mixed quantum classical dynamics, to solve the nonadiabatic dynamics of complex systems<sup>1-41</sup>. The full quantum dynamics methods<sup>7, 8</sup> can give the very accurate description of the nonadiabatic dynamics, while the computational cost is extremely high even unaffordable in complex systems with a huge number of degrees of freedom. The

Gaussian-wavepacket based methods,<sup>12</sup> such as multiple spawning,<sup>11, 42, 43</sup> variational multiconfigurational Gaussians (vMCG)<sup>44-47</sup> and multiconfigurational Ehrenfest,<sup>48, 49</sup> may significantly improve the computational efficiency with keeping reasonable computational accuracy, while a significant amount of computational cost is still required in large systems and numerical implementation also required non-trivial tricks, for instance the proper generation of the new Gaussian wave-packets<sup>43</sup> or the reasonable initial samplings<sup>50</sup>. Several efficient mixed quantum classical approaches, such as Ehrenfest dynamics<sup>20</sup> and its extensions,<sup>51</sup> or trajectory surface-hopping dynamics<sup>5, 6, 13, 24, 37-40</sup>, etc., are very practical in the treatment of the nonadiabatic dynamics of large systems. Thus, great efforts were made to examine the performance of these very efficient methods in various nonadiabatic processes<sup>1, 2, 6, 13, 23, 24, 38-40, 52-57</sup>. At the same time, the on-the-fly versions of these methods are used to simulate the nonadiabatic dynamics of realistic polyatomic systems including all nuclear degrees of freedom<sup>6, 32, 36, 37, 58-63</sup>. However, we should not neglect the deficiencies of these highly approximated methods, such as the improper treatment of electronic coherence and the appearance of frustrated hops in fewest-switches trajectory surface-hopping method<sup>13, 24, 34, 38, 64</sup>.

Meyer and Miller<sup>65</sup> proposed an alternative approach for the theoretical treatment of nonadiabatic dynamics based on mapping discrete quantum states to continuous classical variables. The approach was furtherly revisited by Stock and Thoss in the view of Schwinger's transformation<sup>66</sup>. The resulting MMST (Meyer-Miller-Stock-Thoss) model maps  $N$  discrete quantum states to  $N$  coupled

harmonic oscillator. It is also possible to construct the mapping Hamiltonian by other theoretical approaches<sup>67-72</sup>.

In principle, the MMST mapping approach defines a transformation to construct a mapping Hamiltonian with continuous variables, which may give the equivalent dynamical results with respect to those governed by the original Hamiltonian. Thus, this idea can be combined with different dynamics approaches. For instance, it is possible to combine it with semiclassical initial value representation and its extension<sup>38, 73-84</sup> quantum classical Liouville equation (QCLE)<sup>85-90</sup>, path integral<sup>91-97</sup>, surface hopping<sup>98-101</sup>, centroid molecular dynamics (CMD)<sup>102</sup> and ring-polymer molecular dynamics (RPMD)<sup>103-107</sup>.

The quasi-classical dynamics based on the MMST mapping Hamiltonian (MMST-QC) received considerable interests due to its simplicity<sup>52, 65, 108-119</sup>. Berne and coworkers<sup>52</sup> indicated that the MMST-QC approach outperforms the mean-field dynamics in nonradiative electronic relaxation processes. Stock and Müller<sup>117, 118</sup> introduced the zero-point-energy (ZPE) correction into the MMST-QC approach to solve the ZPE leakage problem. Golosov and Reichman<sup>119</sup> proposed a systematic approach based on the Taylor expansion of the time-dependent observables around  $t=0$ . This idea not only improves the short time performance for the MMST-QC dynamics, but also the long-time one of the dynamics. This way also gives an alternative way to perform the ZPE correction.

In the quasiclassical dynamics procedure, the 'bin' technique has been widely used for the assignment of the final "quantum" states<sup>67, 120-123</sup>. This 'bin' technique

has also been employed to assign the final electronic quantum number in the MMST-QC dynamics<sup>111, 124</sup>. Cotton and Miller<sup>125</sup> proposed that it is more rigorous to perform the window tricks in both the initial sampling and the final assignment of the quantum states in the classical simulations. This gives the so called the symmetrical quasi-classical dynamics method based on the MMST mapping Hamiltonian (MMST-SQC)<sup>126, 127</sup> in which the window width is also relevant to the ZPE correction of the mapping electronic degrees of freedom. In fact, this idea of the double “binning” average procedure appeared in Miller’s earlier work.<sup>128</sup>

Recently, the MMST-SQC method was received much attention and gained significant development.<sup>54-56, 98-101, 126, 127, 129-138</sup> Cotton and Miller<sup>132</sup> proposed a new symmetric windowing technique, triangle windowing technique, for the weak-interstate-coupling cases where original rectangle windowing technique fails. Subotnik and coworkers employed different mixed quantum classical approaches, including the MMST-SQC dynamics, to treat several typical models, such as harmonic and anharmonic systems,<sup>56</sup> bilinear harmonic systems<sup>55</sup> and two-level systems coupled with electromagnetic fields<sup>54</sup>. They indicated that the MMST-SQC method performs well for systems with harmonic bath, while it cannot recover the correct equilibrium populations for systems with anharmonicity<sup>56</sup> that brings the numerical instability associating with “negative forces”. The similar instability problem was noticed in other MMST Hamiltonian based methods<sup>38, 91, 139-141</sup>. Cao, Geva and coworkers<sup>131</sup> modified the MMST-SQC method to treat the anharmonic systems by including the vibrational levels of the anharmonic nuclear modes directly

in the mapping procedure. By using this approach, the modified MMST-SQC method can accurately describe the population dynamics of systems involving anharmonic potential energy surfaces (PESs). Tao developed a few of the extended versions of the MMST-SQC method by combining the MMST-SQC method with the trajectory surface hopping<sup>98-101</sup>. At the same time, the MMST-SQC approach has been applied in several typical situations<sup>126, 127, 133-138</sup>, such as electron transfer<sup>126, 133</sup>, energy transfer<sup>134</sup>, singlet fission<sup>135, 137, 138</sup>, etc.

Overall, the MMST-SQC method is a promising method to treat the nonadiabatic dynamics, thus it is highly interesting to put additional efforts to apply this idea to investigate the nonadiabatic dynamics of more complex systems. Before the formal implementation for the large-scale simulation, it is also necessary to perform the extensive benchmark calculations to give more comprehensive evaluations on the performance of the MMST-SQC method. For this purpose, we try to examine the accuracy of the MMST-SQC method in the dynamics of the spin-boson models used to describe the electron transfer and energy transfer processes in condensed matter systems widely<sup>3, 4</sup>. Particularly, we wish to focus on the performance of MMST-SQC dynamics in the spin-boson systems with different parameters, such as energy gap, electronic couplings, the bath characteristic frequency and electron-phonon coupling. As a benchmark, the full quantum dynamics method, ML-MCTDH, was used to obtain the accurate dynamics results of these model systems for comparison. This work serves as an important complement to the available studies of the MMST-SQC method<sup>54-56, 98-101, 126, 127, 129-138, 142, 143</sup>, before the massive employment of this approach in the treatment of more general nonadiabatic dynamics. This work definitely improves our understanding on the performance of the MMST-SQC method. Because

the spin-boson models with quite different parameters were considered, the current work will give us the direct information on the general performance of the MMST-SQC method, namely in which situation the MMST-SQC dynamics works well. This is certainly useful for the further studies on similar problems.

## 2. THEORY AND METHODS

### 2.1 Hamiltonian

We employed the spin-boson models in this paper, which were widely used to describe the electron transfer and energy transfer processes in previous works<sup>4, 134, 144-146</sup>. Here we mainly consider the spin-boson models that describe the situations of two electronic states (system) coupled with many vibrational modes (bath). A system–bath Hamiltonian including three parts was used to describe the dynamics, namely: the system Hamiltonian  $H_s$  (electronic part) the bath part  $H_b$  (vibrational part) and the system–bath couplings  $H_{sb}$  (electronic-phonon interaction); namely,

$$H = H_s + H_b + H_{sb}, \quad (1)$$

Each part can be further expanded into the following form,

$$\begin{aligned} H_s &= \sum_k |\phi_k\rangle E_k \langle\phi_k| + \sum_{l \neq k} |\phi_k\rangle V_{kl} \langle\phi_l| \\ H_b &= \sum_k \sum_j^{N_b} \frac{1}{2} \omega_{kj} [P_{kj}^2 + Q_{kj}^2] \\ H_{sb} &= \sum_k |\phi_k\rangle \langle\phi_k| \sum_j^{N_b} (-\kappa_{kj} Q_{kj}) \end{aligned}, \quad (2)$$

where  $\phi_k$  and  $\phi_l$  represent the electronic states and  $E_k$  and  $E_l$  are the energies of

the corresponding states.  $V_{kl}$  is the interstate coupling. Each state couples with an individual bath.  $P_{kj}$  and  $Q_{kj}$  are the momentum and position of the  $j$ th mode in the  $k$ th bath coupled with the  $k$ th state. And  $\omega_{kj}$  and  $\kappa_{kj}$  are the frequency and the system-bath coupling constant of the corresponding mode in the diagonal elements of the system Hamiltonian, respectively.  $N_b$  is the bath-mode number. The system-bath couplings for the off-diagonal elements in the system Hamiltonian were neglected. Four different models with various interstate energy gaps and couplings were adopted using the above Hamiltonian.

Here, the continuous Debye-type spectral density<sup>3</sup> was used for bath modes,

$$J(\omega) = \frac{2\lambda\omega\omega_c}{\omega^2 + \omega_c^2}, \quad (3)$$

where  $\omega_c$  is the characteristic frequency of the bath.  $\lambda$  is the reorganization energy representing the coupling strength between system and bath degrees of freedom. Each electronic state was coupled to its corresponding bath. Discrete bath modes were also used to define the spectral density<sup>3</sup>

$$J_k(\omega) = \frac{\pi}{2} \sum_{i=1}^N \kappa_{ki}^2 \delta(\omega - \omega_{ki}). \quad (4)$$

In principle, the continuous spectral density can be discretized to an arbitrary number of bath modes. The coupling coefficient  $\kappa_{ki}$  of each mode is obtained,

$$\kappa_{ki} = \sqrt{\frac{2}{\pi} J_k(\omega_{ki}) \Delta\omega}. \quad (5)$$

when a sampling interval  $\Delta\omega$  was given. The coefficient  $\kappa_{ki}$  stands for the coupling strength of the mode. Normally the electronic-phonon couplings are well characterized by the reorganization energy, or the values of the coupling strength

divided by the frequency of the corresponding mode. In the discretization of the bath modes, different bath mode number gives different coupling strength  $\kappa_{ki}$  for the modes in the same frequency domains. Thus, it is not straightforward to employ the coupling strength to represent the system-bath couplings in the current situation. Instead, we employed a rather simple and direct approach here. Let us assume that the bath organization energy is represented by the single mode with the characteristic frequency, then we can define  $\kappa/\omega_c$ ,

$$\kappa/\omega_c = \sqrt{\frac{2\lambda}{\omega_c}}, \quad (6)$$

to characterize electron-phonon coupling strength of the bath.

## 2.2 Symmetry-Quasi-Classical Dynamics Method Based on Mapping Hamiltonian

The  $\hat{H}$  is used as Hamiltonian of a  $N$ -state system

$$\hat{H} = \sum_{k,l} \hat{h}_{kl} |\phi_k\rangle\langle\phi_l|, \quad (7)$$

where  $\phi_k$  and  $\phi_l$  denote the quantum states of the system. The diagonal element  $\hat{h}_{kk}$  represents the energy operator (kinetic and potential energies). The off-diagonal element  $\hat{h}_{kl}$  ( $k \neq l$ ) denotes the interstate coupling operator. This Hamiltonian is represented in the discrete quantum-state basis ( $\phi_k$ ). The main idea of the mapping approach is to map the discrete representation to a continuous one.

In the MMST model<sup>127</sup>, a  $N$ -state system is mapped to a  $N$  coupled harmonic

oscillators. The annihilation operator  $\hat{a}_k$  and the creation operator  $\hat{a}_l^+$  were used to construct the mapping relation, namely

$$\begin{aligned} |\phi_k\rangle\langle\phi_l| &\mapsto \hat{a}_k^+\hat{a}_l, \\ |\phi_k\rangle &\mapsto |0_1 \cdots 1_k \cdots 0_N\rangle. \end{aligned} \quad (8)$$

The relationship between the annihilation operator and the creation operator is given as  $[\hat{a}_k, \hat{a}_l^+] = \delta_{kl}$ . When the Cartesian coordinate operator  $\hat{x}_k = (\hat{a}_k^+ + \hat{a}_k)/\sqrt{2}$  and the momentum operator  $\hat{p}_k = i(\hat{a}_k^+ - \hat{a}_k)/\sqrt{2}$  of the harmonic oscillator were introduced, the MMST Hamiltonian  $\hat{H}$  is written as

$$\hat{H} = \sum_k \frac{1}{2} (\hat{x}_k^2 + \hat{p}_k^2 - 1) \hat{h}_{kk} + \frac{1}{2} \sum_{k \neq l} (\hat{x}_k \hat{x}_l + \hat{p}_k \hat{p}_l) \hat{h}_{kl}, \quad (9)$$

A purely classical mapping Hamiltonian can be obtained by substituting the quantum operators with their corresponding physical variables in the MMST Hamiltonian, namely

$$H_{MM}(x, p, Q, P) = \sum_k \frac{1}{2} (x_k^2 + p_k^2 - \gamma) H_{kk}(Q, P) + \frac{1}{2} \sum_{k \neq l} (x_k x_l + p_k p_l) H_{kl}(Q, P), \quad (10)$$

where  $x_k$  and  $p_k$  are the classical coordinates and momenta for the quantum-state part.  $Q$  and  $P$  are the coordinates and momenta of the environmental part.  $H_{kk}$  and  $H_{kl}$  are the classical correspondences of the quantum Hamiltonian matrix elements.  $\gamma$  is a parameter accounting for the effective zero-point energy. It is possible to perform the proper initial sampling and run the classical dynamics over many trajectories starting from this classical mapping Hamiltonian, which provides a quasi-classical trajectory-based approach to treat the nonadiabatic dynamics.

In the quasi-classical dynamics, the distribution of final quantum states (occupation) can be obtained by calculating the final values of the action variables  $n_k = \frac{1}{2} \left( (x^{(k)})^2 + (p^{(k)})^2 - \gamma \right)$  accumulated in “bins” (or histograms) centered at quantum occupation values  $N = 0$  or  $1$ . Cotton and Miller proposed that the “bin” idea should be employed for both initial-state sampling and final-state assignment<sup>127</sup>, giving the so-called symmetrical quasiclassical (SQC) dynamics. In the SQC method, the “window functions”  $W_k$  is defined as

$$W_k(n_k, N) = \frac{1}{\Delta n} h\left(\frac{\Delta n}{2} - |n_k - N|\right), \quad (11)$$

where  $h(z)$  is the Heaviside function,  $h(z) = 0$  when  $z < 0$  and  $h(z) = 1$  when  $z \geq 0$ .  $\Delta n$  is the window width and  $\Delta n = \gamma$  is recommended in the MMST-SQC method.<sup>136</sup>

In the MMST-SQC dynamics simulations, the initial-state sampling can be performed using the action-angle sampling method, namely

$$\begin{aligned} x_k &= \sqrt{2n_k + \gamma} \cos \theta \\ p_k &= \sqrt{2n_k + \gamma} \sin \theta \end{aligned} \quad (12)$$

where  $n_k \in [N - \Delta n/2, N + \Delta n/2]$  ( $N = 0$  or  $1$ ) and the angle  $\theta \in [-\pi, \pi)$ . For the final states, the same binning way is also performed for the assignment of the quantum state. The time-dependent populations  $P_{map,k}$  of electronic states are evaluated by averaging over all trajectories

$$P_{map,k}(t) = \frac{\left\langle \left[ W_i(n_i(0),1) \prod_{l \neq i} W_l(n_l(0),0) \right] \left[ W_k(n_k(t),1) \prod_{l \neq k} W_l(n_l(t),0) \right] \right\rangle}{\sum_m \left\langle \left[ W_i(n_i(0),1) \prod_{l \neq i} W_l(n_l(0),0) \right] \left[ W_m(n_m(t),1) \prod_{l \neq m} W_l(n_l(t),0) \right] \right\rangle} \quad (13)$$

### 2.3 ML-MCTDH

In the traditional quantum wavepacket dynamics, a group of time-independent bases for each primary coordinate is used to represent the wavefunction, only the time-dependent coefficients evolving with time. The MCTDH method, instead, employs the time-dependent bases to represent wavefunction. The equations of motion of the coefficients and the basis functions can be obtained by the variational principle <sup>7</sup>.

The ML-MCTDH approach is an extension of the standard MCTDH method. The wavefunction is represented by a multilayer tree structure, which is expanded by the multi-dimensional basis functions recursively until the time-independent bases of each primary coordinate are reached. In principle, the ML-MCTDH provides the numerically accurate simulation of the quantum dynamics of complex systems. The expansion of tree structure has a great influence on the computational convergence and efficiency. The principle for the construction of tree structure has been discussed in detail in the previous works <sup>4, 144, 145, 147, 148</sup>, which will not be restated here. In this work, ML-MCTDH calculations were conducted to get the accurate dynamical results for benchmark.

## 2.4 Computational Details

Since we built the models for charge and energy transfer problems, we name the initial state as the donor state in the whole context. In the current spin-boson model, the second state is the acceptor state. Here we also assume that both electronic states are excited states each of which is coupled to an individual bath. According to the Condon approximation, the initial state is obtained by placing the lowest vibrational level of the ground electronic state into the donor state in both the ML-MCTDH and MMST-SQC calculations.

The ML-MCTDH calculations were performed using the Heidelberg MCTDH package.<sup>149</sup> It is well known the ML-MCTDH calculations are easily performed at the zero temperature. Because many works have already check the performance of the MMST-SQC method at the finite temperature<sup>54-56, 126, 127, 134, 135, 137, 138</sup>, we decide to mainly focus on the case with zero temperature. Thus, as discussed in the previous paragraph, the initial nuclear wavefunction is obtained as the lowest vibrational level of the ground electronic state. Then we put it into the donor state. Such types of models are discussed in the previous review<sup>4</sup>. Please notice that the current initial condition gives the non-equilibrium nuclear density for the donor electronic state.

In the MMST-SQC calculations, the ZPE correction  $\gamma = 0.732$  was considered<sup>136</sup> for the electronic degrees, indicating that the window width of the initial sampling of freedom is 0.732.

For the nuclear degrees of freedom, the Wigner sampling was used in most cases. In order to check the dependence of the MMST-SQC dynamics on the different initial samplings of the nuclear degrees of freedom, the initial sampling for the bath modes

was also conducted by using the action-angle sampling method with various ZPE corrections and window widths in a few of additional calculations.

### 3. RESULTS

Four groups of the spin-boson models with various energy gaps and inter-state couplings were considered in this work. The first two groups of the spin-boson models with small inter-state coupling (0.0124 eV) mimic the situations of the photoinduced energy transfer in photoharvesting systems<sup>134, 150</sup>. To check the performance of the MMST-SQC dynamics in symmetric and asymmetric systems, the inter-state energy gap is chosen to be 0 and 0.0124 eV for the first and the second groups of the spin-boson models, respectively. The other two groups of the spin-boson models take large inter-state coupling 0.1 eV that is a typical one in the photoinduced charge transfer processes in organic solar cells<sup>4, 145, 146, 151, 152</sup>. Two inter-state energy gaps, 0.1 and 0.2 eV, are considered in the third and the fourth groups of the spin-boson models.

We took baths with the different characteristic frequencies and the various electron-phonon coupling strengths to check the performance of the MMST-SQC method with respect to the ML-MCTDH results as benchmarks. The characteristic frequencies  $\omega_c$  of the baths cover the range from 40 to 3000  $\text{cm}^{-1}$  and the parameter  $\kappa/\omega_c$  characterizing electron-phonon coupling strength of the bath is chosen as 0.3, 0.5, 0.7 or 1.0.

The main purpose of this work is to compare the results obtained by both the ML-MCTDH and MMST-SQC calculations. As long as the same Hamiltonian is used in both two dynamical calculations, such comparison becomes meaningful. The current work employed 100 modes to represent the continuous bath. In this way, both two dynamical methods employed the identical Hamiltonian. This fully satisfies the purpose of the current work. In this sense, we do not worry whether the current discretization gives the enough number of the bath modes to represent the true bath or not, because this does not affect the main results of the current work.

### **3.1 Symmetric Spin-Boson models with Weak Diabatic Couplings**

The first group of the spin-boson models included several symmetric ones with  $\Delta E = 0$  and  $V_{12} = 0.0124$  eV. The results of MMST-SQC and ML-MCTDH are shown in Figure 1. When the characteristic frequency is low and the electron-phonon coupling is weak, we see the clear oscillation pattern in the time-dependent population dynamics. Such oscillation is governed by the electronic coherent dynamics and its amplitude decays slowly with time being. When the characteristic frequency of the bath increases or the electron-phonon coupling gets stronger, the oscillation amplitude of the time-dependent electronic population in the ML-MCTDH dynamics becomes weaker. As expected, in the cases with strong electron-phonon couplings and the high characteristic frequencies of the bath, the population oscillation vanishes and a monotonic population decay is observed.

In previous works<sup>153</sup>, the ratio between the electronic coupling and the characteristic frequency of the bath  $V_{12}/\omega_c$  was used to classify the electron transfer reactions into three regions, i.e., adiabatic (slow bath) region ( $V_{12}/\omega_c \gg 1$ ), nonadiabatic (fast bath) region ( $V_{12}/\omega_c \ll 1$ ) and intermediate region ( $V_{12}/\omega_c \approx 1$ ).

In the adiabatic and intermediate regions ( $\omega_c = 40, 100, 200 \text{ cm}^{-1}$  and  $V_{12}/\omega_c \leq 2$ ), the MMST-SQC method give results very close to the ML-MCTDH ones, and even in some cases the identical results are obtained (Figure 1).

In the nonadiabatic region, the MMST-SQC results deviate from the ML-MCTDH ones. The population recurrences become weaker and vanishes more quickly in the MMST-SQC calculations than those in the ML-MCTDH results in the weak electron-phonon coupling ( $\kappa/\omega_c = 0.3$  and  $0.5$ ) models. With intermediate electron-phonon coupling ( $\kappa/\omega_c = 0.7$ ), the MMST-SQC dynamics display the monotonic decay patterns instead of the weak population oscillations in the ML-MCTDH dynamics. In the strong electron-phonon coupling ( $\kappa/\omega_c = 1.0$ ) models, the monotonic population decay in the MMST-SQC dynamics is slower than that in the ML-MCTDH dynamics. The quicker damping of the population oscillation also appears in the previous study of nonradiative electronic relaxation by the MMST-QC (without windowing) dynamics<sup>52</sup>. Moreover, the discrepancy between the ML-MCTDH and MMST-SQC results becomes larger with the electron-phonon coupling increasing in the nonadiabatic bath region. The dependence of the accuracy of the MMST-SQC dynamics on the Hamiltonian was also discussed by Subotnik and coworkers<sup>55, 56</sup>.

Overall, the MMST-SQC method provides reasonable results in these symmetric models, except for some models with rather high characteristic frequencies of the bath and strong electron-phonon couplings.

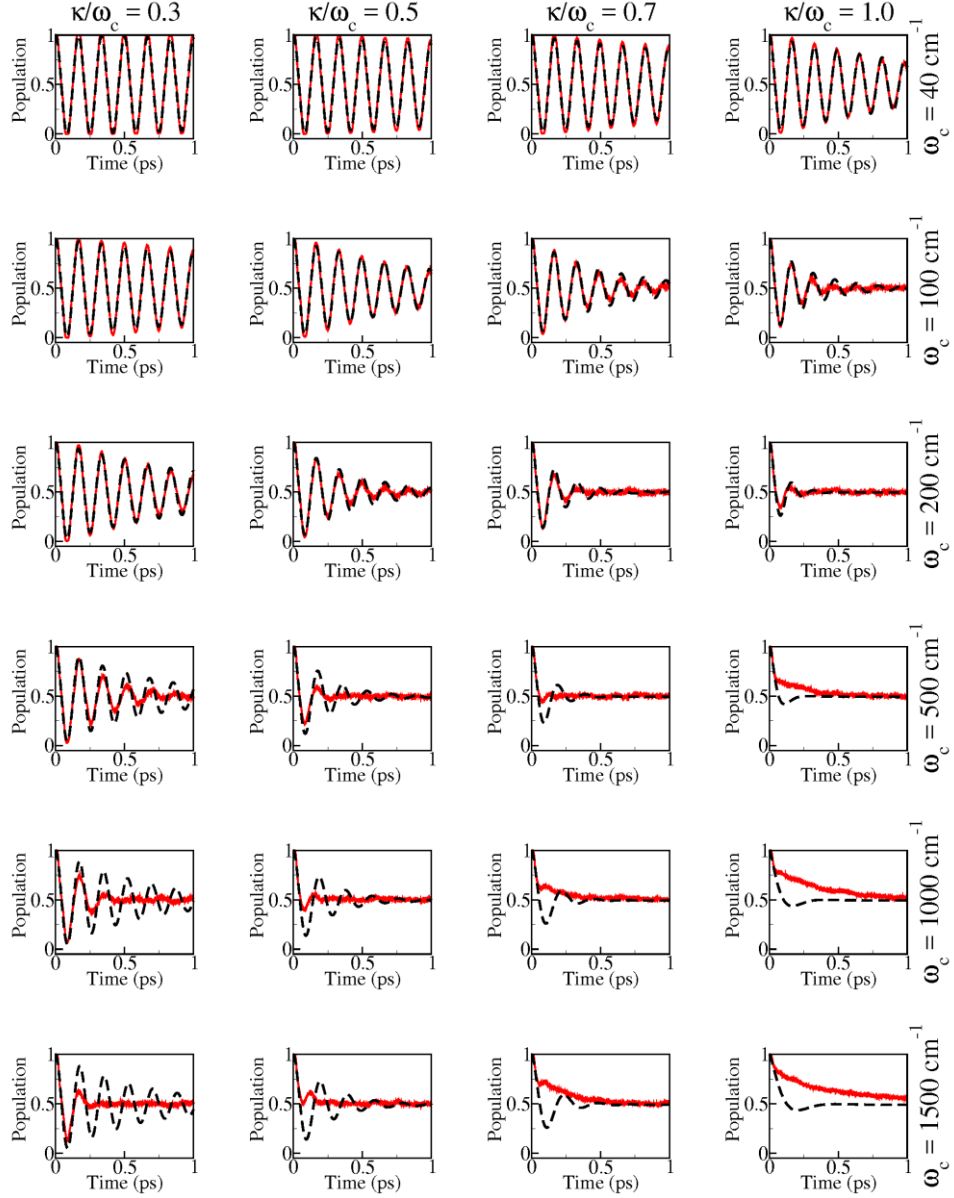


Figure 1. Time-dependent electronic population (or occupation) of the donor state in various two-state models with  $\Delta E = 0$  and  $V_{12} = 0.0124$  eV. The characteristic bath frequencies  $\omega_c$  are 40, 100, 200, 500, 1000 and 1500  $\text{cm}^{-1}$  and the electron-phonon coupling strength of the baths,  $\kappa/\omega_c$ , are 0.3, 0.5, 0.7 and 1.0. Black dashed lines denote the ML-MCTDH results. Red solid lines denote the MMST-SQC results.

### 3.2 Asymmetric Spin-Boson Models with Weak Diabatic Couplings

A series of asymmetric models with the same parameters as the symmetric models above were built except the energy gap  $\Delta E = 0.0124$  eV. The dynamical results are shown in Figure 2. In the ML-MCTDH results, the overall population evolution of the donor state in the asymmetric models is very similar to that in the symmetric models, except that different population plateaus are reached at the end. Because of the higher energy of the initial donor state, the final population of the donor state tends to be less than 0.5 at the end of the ML-MCTDH simulation.

The MMST-SQC results are also generally consistent with the ML-MCTDH ones in the adiabatic and intermediate bath regions for these asymmetric models. In nonadiabatic bath region, the deviations exist between two different dynamics calculation results and the population oscillation becomes weaker in the MMST-SQC dynamics. In the models with rather high characteristic frequencies of the bath and strong electron-phonon couplings, the populations do not match at the end of simulation time. Miller and Cotton<sup>129</sup> once pointed out that the detailed balance “in principle” should be satisfied in the MMST-SQC dynamics. Subotnik and coworkers<sup>56</sup> also showed the good performance of the MMST-SQC method when the system accesses the thermal equilibrium limit in the harmonic cases. Thus, it is not fully known whether the MMST-SQC dynamics gives the correct values of population dynamics in the longer simulation time. However, we do not focus on such issue here because the main purpose of this work is to examine the performance of the MMST-SQC dynamics in the treatment of ultrafast dynamics.

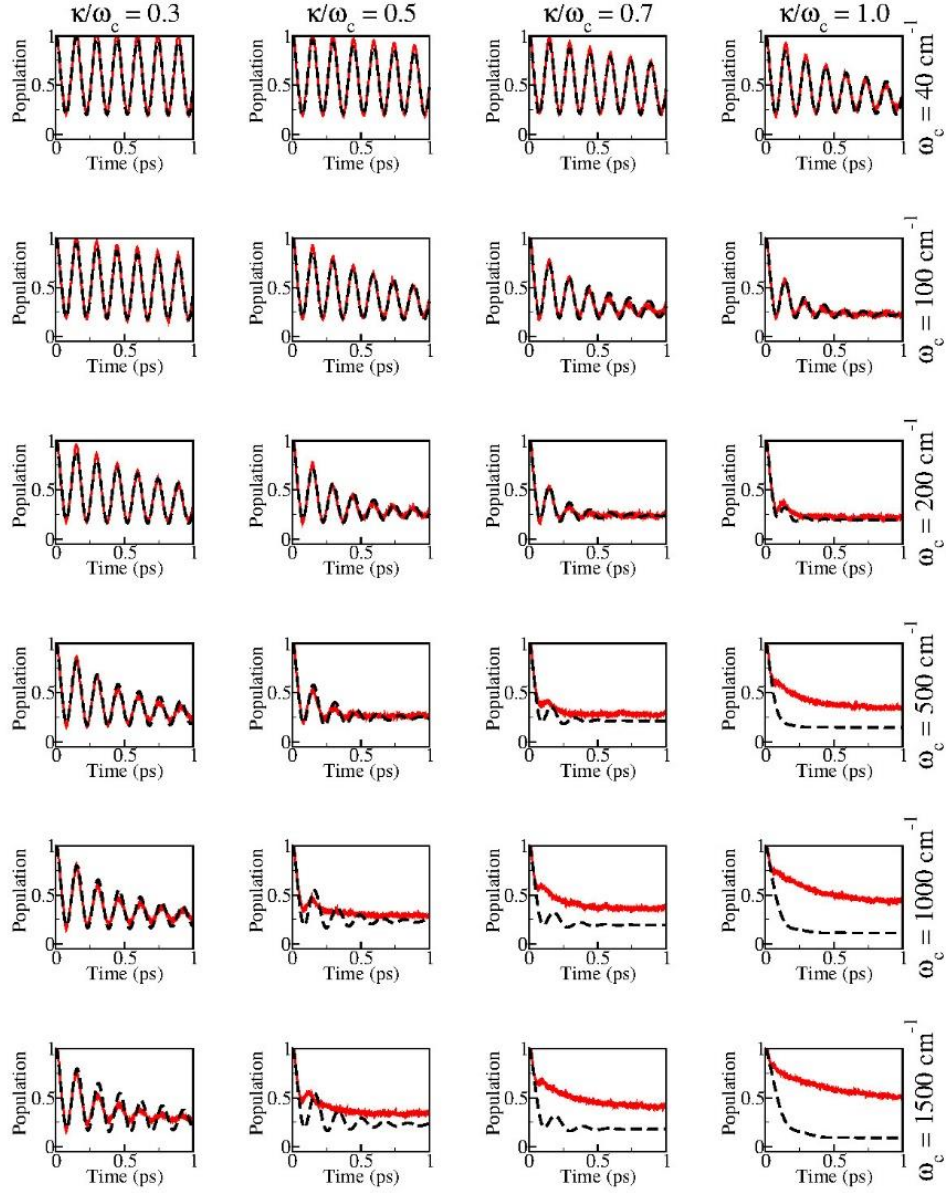


Figure 2. Time-dependent electronic population (or occupation) of the donor state in various spin-boson models with  $\Delta E = V_{12} = 0.0124$  eV. The characteristic bath frequencies  $\omega_c$  are 40, 100, 200, 500, 1000 and 1500  $\text{cm}^{-1}$  and the electron-phonon coupling strength of the baths,  $\kappa/\omega_c$ , are 0.3, 0.5, 0.7 and 1.0. Black dashed lines denote the ML-MCTDH results. Red solid lines denote the MMST-SQC results.

### 3.3 Asymmetric Spin-Boson Models with Strong Diabatic Couplings

Previous models with small inter-state coupling takes parameter values that were used in the discussions of photoinduced intermolecular energy transfer process in photoharvesting systems<sup>134, 150</sup>. In some typical photoinduced charge transfer processes in organic solar cells, the inter-state energy gaps and couplings sometimes may be larger<sup>4, 145, 146, 151, 152</sup>. Thus, two additional types of asymmetric models with  $\Delta E = V_{12} = 0.1$  eV and  $\Delta E = 2V_{12} = 0.2$  eV were used to check the performance of the MMST-SQC method, see Figure 3 ( $\Delta E = V_{12} = 0.1$  eV) and Figure 4 ( $\Delta E = 2V_{12} = 0.2$  eV).

Due to the larger inter-state energy gap and the stronger electronic coupling, much faster system dynamics was observed compared to those of the first two types of the spin-boson models. Thus, we only provided the population evolution within the first 100 fs. For all models, the MMST-SQC results are close to the ML-MCTDH ones even when the bath displays the high characteristic frequencies. The good performance of the MMST-SQC method here is attributed the fact that the fast electronic motion indicates that the bath motion becomes comparably slower in these models. The continuous rising of bath frequencies may lead to the inaccurate results of the MMST-SQC dynamics. However, the bath with the very high characteristic frequency should not exist in some realistic situations, such as photoinduced energy transfer and charge transfer processes in organic photovoltaic systems. Only the stretching motions involving the H atoms, such as the OH, CH stretching motions, display such high vibrational frequency  $> 3000$  cm<sup>-1</sup>, while these motions normally

display very small electron-phonon coupling in these processes<sup>4</sup>, and should not play an essential role in photoinduced energy/charge transfer in organic photovoltaic systems.

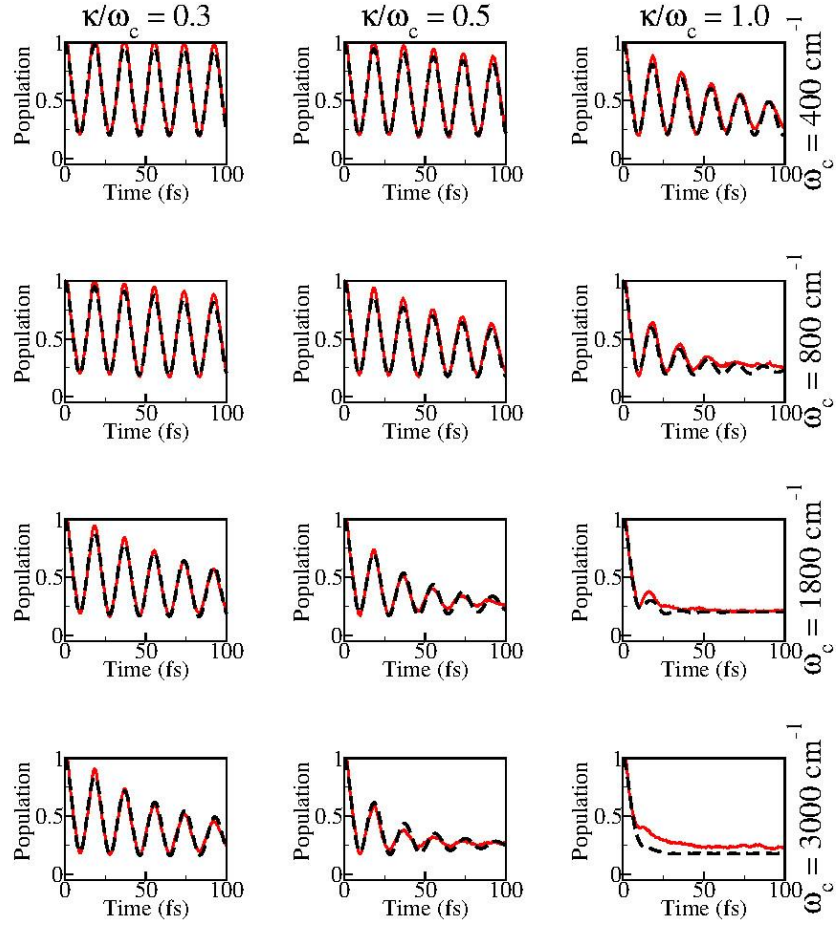


Figure 3. Time-dependent electronic population (or occupation) of the donor state in various two-state models with  $\Delta E = V_{12} = 0.1$  eV. The characteristic bath frequencies  $\omega_c$  are 400, 800, 1800 and 3000  $\text{cm}^{-1}$  and the electron-phonon coupling strength of the baths,  $\kappa/\omega_c$ , are 0.3, 0.5 and 1.0. Black dashed lines denote the ML-MCTDH results. Red solid lines denote the MMST-SQC results.

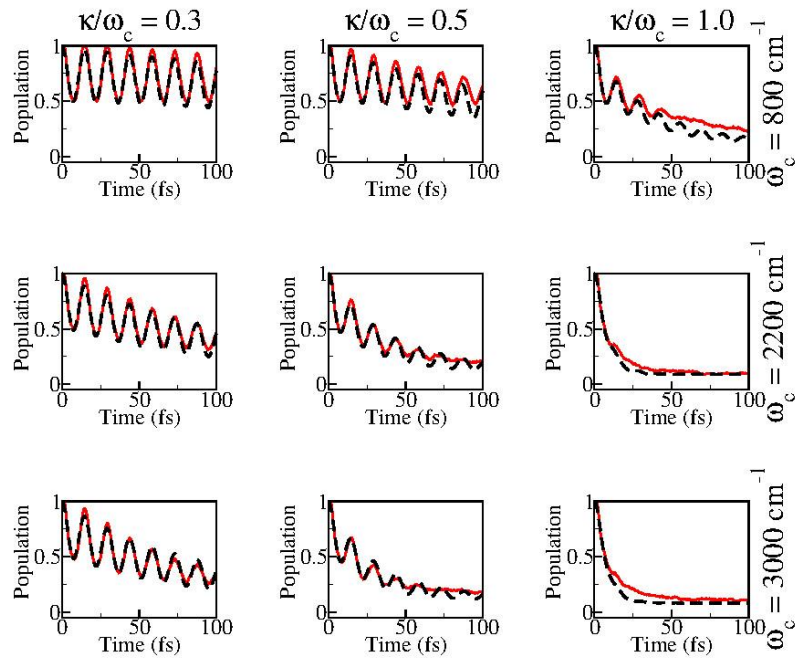


Figure 4. Time-dependent electronic population (or occupation) of the donor state in various two-state models with  $\Delta E = 0.2$  eV and  $V_{12} = 0.1$  eV. The characteristic bath frequencies  $\omega_c$  are 800, 2200 and 3000  $\text{cm}^{-1}$  and the electron-phonon coupling strength of the baths,  $\kappa/\omega_c$ , are 0.3, 0.5 and 1.0. Black dashed lines denote the ML-MCTDH results. Red solid lines denote the MMST-SQC results.

### 3.4 Initial Sampling of the Nuclear Configurations

The MMST mapping procedure involves the transformation between the quantum occupation number of the harmonic oscillator and the physical variables (coordinate and momentum), which can also be written in the action-angle format. Thus, it is rather logical to employ the action-angle initial sampling for the mapping electronic degrees of freedom. However, for the nuclear degrees of freedom, there is no strict rule to provide such the quantum-classical correspondence. As a result, different ways may be employed for the initial sampling of the nuclear degrees of freedom, which mimic the corresponding quantum distribution. We noticed that many works on the MMST-SQC dynamics employed the Wigner sampling for the nuclear degrees of freedom, particular in the cases with finite temperature<sup>55, 56, 126, 127, 131, 133, 136, 137</sup>. Along this line, most of our calculations also employed the Wigner sampling for the bath modes. Certainly, it is also possible to perform the action-angle sampling for the nuclear modes. We thus try to consider different ways of the initial samplings for the nuclear degrees of freedom, including the Wigner sampling, the action angle samplings with different windows and the ZPE correction.

For the above symmetric spin-boson models, we observed that the Wigner sampling and the action-angle sampling ( $\gamma_{\text{nuc}} = 1.0$ ) methods give very similar results in the MMST-SQC dynamics, see Figure 5. Only when the ZPE correction employs small value of  $\gamma_{\text{nuc}}=0.4$ , the action-angle sampling gives slightly different results in the the strong electronic-phonon coupling cases, particular for the baths with high characteristic frequencies. Overall, different initial sampling approaches

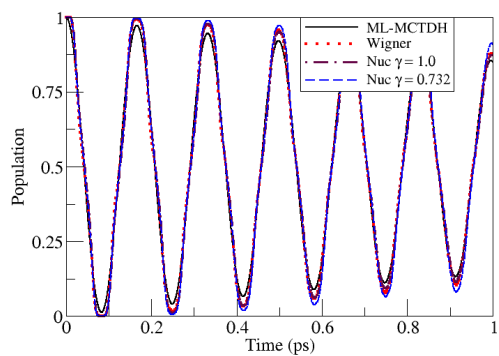
employed here seem not improve the performance of the MMST-SQC dynamics for the symmetrical spin-boson models.

For the asymmetric spin-boson models, we have seen that obvious different results exist between the MMST-SQC and ML-MCTDH dynamics when the fast bath is considered. Thus, we mainly discuss this situation here by employing a typical example with  $\omega_c = 1000 \text{ cm}^{-1}$  (Figure 6). In these cases, the Wigner sampling and the action-angle sampling without the ZPE correction ( $\gamma_{\text{nuc}} = 1.0$ ) for the nuclear degrees of freedom give very similar results. However, in the current asymmetric spin-boson models, the inclusion of the ZPE correction for the nuclear degrees of freedom in the initial sampling improves the performance of the MMST-SQC dynamics. The simulation results are dependent on the  $\gamma_{\text{nuc}}$  value. The lower  $\gamma_{\text{nuc}}$  values seem to give the lower donor-state population, particularly for the long-time dynamics. We also noticed that the smaller ZPE correction should be employed for the strong electronic-phonon coupling cases.

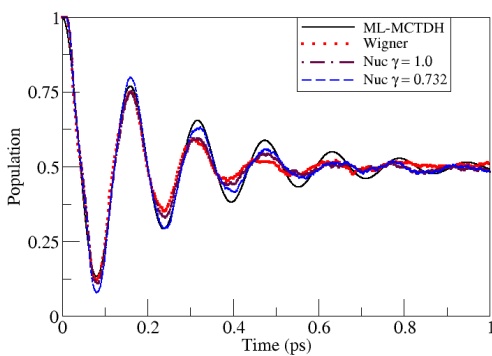
According to the above observations, we realized that the influence of the initial sampling for the nuclear degrees of freedom is rather complicated. The MMST-SQC dynamics seems not significantly depend on whether the Wigner sampling or the action angle sampling without the ZPE correction is used in the initial sampling of nuclear degrees of freedom. When the ZPE correction is employed, different results are found in symmetric and asymmetric spin boson models. The ZPE correction in the initial sampling of the nuclear degrees of freedom seems not give the very deep impact on the overall dynamics in the symmetric spin-boson models, while the ZPE

correction with different  $\gamma_{\text{nuc}}$  value substantially changes the MMST-SQC dynamics in the asymmetric spin-boson models.

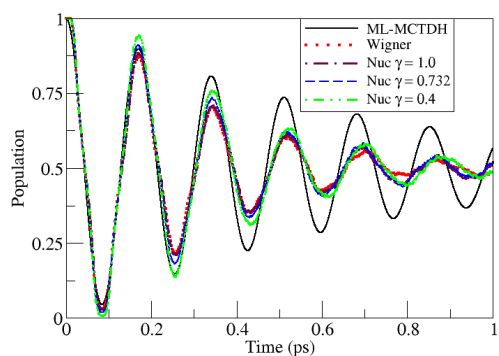
Overall, the dependence of the nonadiabatic dynamics on the ZPE correction for the initial sampling of the nuclear degrees of freedom seems to be highly dependent on the system models. The current study mainly focuses on the performance of the MMST-SQC dynamics, thus the deep understanding of the ZPE corrections is beyond the scope of this work. In fact, the research on the ZPE correction in the classical simulation is an extremely challenging topic<sup>117, 118, 154-157</sup>.



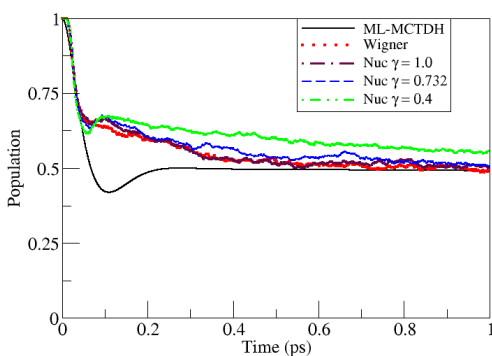
(a)  $\omega_c = 100 \text{ cm}^{-1}$ ,  $\kappa/\omega_c = 0.3$



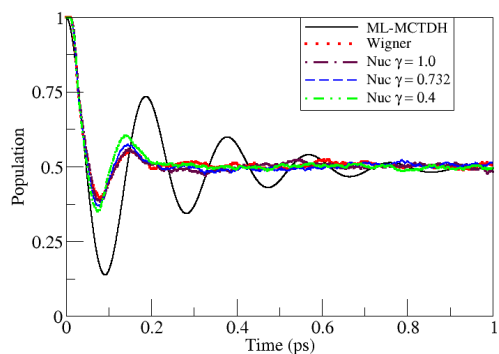
(b)  $\omega_c = 100 \text{ cm}^{-1}$ ,  $\kappa/\omega_c = 1.0$



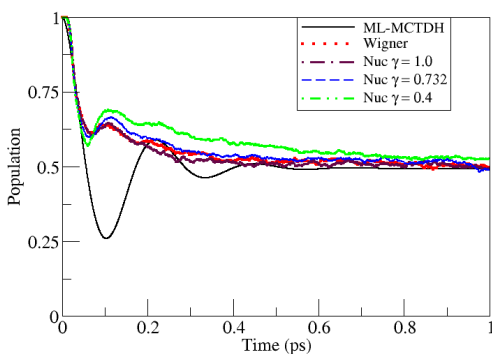
(c)  $\omega_c = 500 \text{ cm}^{-1}$ ,  $\kappa/\omega_c = 0.3$



(d)  $\omega_c = 500 \text{ cm}^{-1}$ ,  $\kappa/\omega_c = 1.0$



(e)  $\omega_c = 1000 \text{ cm}^{-1}$ ,  $\kappa/\omega_c = 0.5$



(f)  $\omega_c = 1000 \text{ cm}^{-1}$ ,  $\kappa/\omega_c = 0.7$

Figure 5. Time-dependent electronic population (or occupation) of the donor state in a two-state model with  $\Delta E = 0$  and  $V_{12} = 0.0124 \text{ eV}$ .

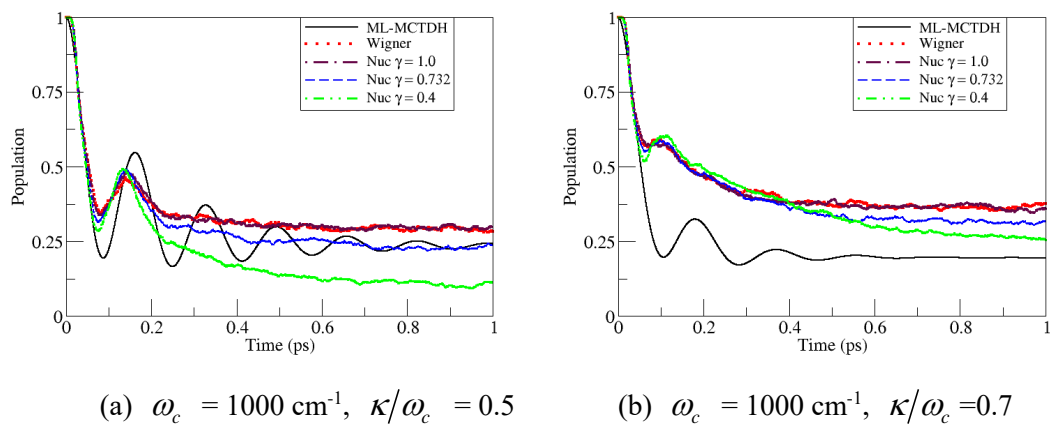


Figure 6. Time-dependent electronic population (or occupation) of the donor state in a two-state model with  $\Delta E = V_{12} = 0.0124 \text{ eV}$ .

## 4. CONCLUSION

The performance of the MMST-SQC method was extensively examined by employing four types of the spin-boson models representing the photoinduced charge/energy transfer processes. These models consider different Hamiltonian parameters, such as energy gap, electronic coupling, the bath characteristic frequency and electron-phonon coupling. The ML-MCTDH method was used to benchmark the results obtained from the MMST-SQC dynamics. For the first two types of the spin-boson models with weak electronic coupling, 0.0124 eV, the MMST-SQC method performs very well in the low-characteristic-frequency and weak-electron-phonon-coupling regions, and it even provides the identical results as those of the ML-MCTDH method. When increasing the characteristic frequency and electron-phonon coupling, the deviations from the ML-MCTDH results are observed. In the third and fourth groups of models strong electronic coupling 0.1 eV is considered and the electronic motion becomes faster, the “fast bath” in the first two groups of the spin-boson models becomes the comparably slow in the last two groups of the spin-boson models with strong electronic couplings. As the result, the MMST-SQC method can produce results consistent with the exact ML-MCTDH results in many models, while the deviations are observed when the characteristic frequency of the bath is extremely high and the electron-phonon couplings are very strong.

The dependence of the MMST-SQC dynamics on the initial sampling of the nuclear degrees of freedom is also addressed. It is important to noticed that the Winger sampling and action angle sampling without the ZPE correction give the very similar results, no matter whether the symmetric or asymmetric spin-boson models are

considered. In the action angle sampling, we still miss the comprehensive understanding of the possible effects of the ZPE correction for the nuclear degrees of freedom on the overall nonadiabatic dynamics. For example, different  $\gamma_{\text{nuc}}$  value gives rather different population dynamics in the asymmetric spin-boson models, while such dependence seems to be minor in the symmetric spin-boson models. Thus, more further efforts should be devoted to understand the ZPE problem of the nuclear degrees of freedom in the MMST-SQC dynamics.

Overall, the MMST-SQC method performs well in many of our testing spin-boson models corresponding to photoinduced charge/energy processes in photoharvesting systems and organic solar cells. Particularly, when the slow bath or the weak system-bath interactions are involved, this method gives very accurate results. Thus, the MMST-SQC method is quite promising to treat the nonadiabatic dynamics of the complex systems within the the similar parameter regions discussed in this work. At the same time, it should be also highly interesting to combine it with the on-the-fly dynamics. However, as discussed by some works<sup>54, 56</sup>, the numerical instability may appear in the MMST-SQC dynamics when the anharmonic potential appears. This is also a very challenging topic in the future.

## **AUTHOR INFORMATION**

### **Corresponding Author**

\* [E-mail: lanzg@qibebt.ac.cn; zhenggang.lan@gmail.com](mailto:lanzg@qibebt.ac.cn)

Fax: +86-532-80662778; Tel: +86-532-80662630.

## Notes

The authors declare no competing financial interest.

## ACKNOWLEDGEMENTS

This work is supported by NSFC projects (Nos. 21673266, 21503248 and 11747170). Z. L. thanks the support by the Natural Science Foundation of Shandong Province for Distinguished Young Scholars (JQ201504). J. Z. thanks the Natural Science Foundation of Shandong Province (ZR2018BB043) and the Postdoctoral Scientific Research Foundation of Qingdao (2017012). The authors thank the Supercomputing Center; Computer Network Information Center, CAS; National Supercomputing Center in Shenzhen; National Supercomputing Center in Guangzhou and the Supercomputing Center of CAS-QIBEBT for providing computational resources.

## REFERENCE

1. W. Domcke, D. R. Yarkony and H. Köppel, *Conical intersections: theory, computation and experiment*. (World Scientific, 2011).
2. W. Domcke, D. R. Yarkony and H. Köppel, *Conical Intersections: Electronic Structure, Dynamics and Spectroscopy*. (World Scientific, Singapore, 2004).
3. V. May and O. Kühn, *Charge and Energy Transfer Dynamics in Molecular Systems*. (Wiley-VCH Verlag GmbH & Co., KGaA, Boschstr. 12, 69469 Weinheim, Germany, 2011).
4. M. Schroter, S. D. Ivanov, J. Schulze, S. P. Polyutov, Y. Yan, T. Pullerits and O.

- Kühn, *Phys. Rep.* **567**, 1-78 (2015).
5. J. C. Tully, *J. Chem. Phys.* **93** (2), 1061-1071 (1990).
  6. R. Crespo-Otero and M. Barbatti, *Chem. Rev.*, DOI: 10.1021/acs.chemrev.1027b00577 (2018).
  7. M. H. Beck, A. Jackle, G. A. Worth and H. D. Meyer, *Phys. Rep.* **324** (1), 1-105 (2000).
  8. H. B. Wang and M. Thoss, *J. Chem. Phys.* **119** (3), 1289-1299 (2003).
  9. L. Han, Y. L. Ke, X. X. Zhong and Y. Zhao, *Int. J. Quantum Chem.* **115** (9), 578-588 (2015).
  10. L. P. Chen, R. H. Zheng, Q. Shi and Y. J. Yan, *J. Chem. Phys.* **131** (9), 094502 (2009).
  11. M. Ben-Nun and T. J. Martínez, *J. Chem. Phys.* **112** (14), 6113-6121 (2000).
  12. B. F. E. Curchod and T. J. Martínez, *Chem. Rev.* **118** (7), 3305-3336 (2018).
  13. J. E. Subotnik, A. Jain, B. Landry, A. Petit, W. J. Ouyang and N. Bellonzi, *Annu. Rev. Phys. Chem.* **67**, 387-417 (2016).
  14. T. Yonehara, K. Hanasaki and K. Takatsuka, *Chem. Rev.* **112** (1), 499-542 (2012).
  15. M. F. Herman, *J. Phys. Chem. A* **109** (41), 9196-9205 (2005).
  16. Q. Shi and E. Geva, *J. Chem. Phys.* **121** (8), 3393-3404 (2004).
  17. M. Barbatti, G. Granucci, M. Persico, M. Ruckebauer, M. Vazdar, M. Eckert-Maksic and H. Lischka, *J Photoch Photobio A* **190** (2-3), 228-240 (2007).
  18. R. Kapral and G. Ciccotti, *J. Chem. Phys.* **110** (18), 8919-8929 (1999).
  19. K. Saita and D. V. Shalashilin, *J. Chem. Phys.* **137** (22), 22A506 (2012).
  20. X. Li, J. C. Tully, H. B. Schlegel and M. J. Frisch, *J. Chem. Phys.* **123** (8), 084106 (2005).
  21. M. J. Bedard-Hearn, R. E. Larsen and B. J. Schwartz, *J. Chem. Phys.* **123** (23), 234106 (2005).
  22. C. Y. Zhu, A. W. Jasper and D. G. Truhlar, *J. Chem. Theory Comput.* **1** (4), 527-540 (2005).
  23. A. V. Akimov, A. J. Neukirch and O. V. Prezhdo, *Chem. Rev.* **113** (6), 4496-4565 (2013).
  24. L. J. Wang, A. Akimov and O. V. Prezhdo, *J. Phys. Chem. Lett.* **7** (11), 2100-2112 (2016).
  25. S. K. Min, F. Agostini, I. Tavernelli and E. K. U. Gross, *J. Phys. Chem. Lett.* **8** (13), 3048-3055 (2017).
  26. J. E. Subotnik, *J. Chem. Phys.* **132** (13), 134112 (2010).
  27. Y. Yao, K.-W. Sun, Z. Luo and H. Ma, *J. Phys. Chem. Lett.* **9** (2), 413-419 (2018).
  28. V. N. Gorshkov, S. Tretiak and D. Mozyrsky, *Nat. Commun.* **4**, 2144 (2013).
  29. F. Webster, E. T. Wang, P. J. Rossky and R. A. Friesner, *J. Chem. Phys.* **100** (7), 4835-4847 (1994).
  30. A. K. Belyaev, C. Lasser and G. Trigila, *J. Chem. Phys.* **140** (22), 224108 (2014).
  31. N. Shenvi, J. E. Subotnik and W. T. Yang, *J. Chem. Phys.* **134** (14), 144102 (2011).
  32. E. Tapavicza, I. Tavernelli and U. Rothlisberger, *Phys. Rev. Lett.* **98** (2), 023001 (2007).

33. J. Y. Fang and S. Hammes-Schiffer, *J. Phys. Chem. A* **103** (47), 9399-9407 (1999).
34. G. Granucci and M. Persico, *J. Chem. Phys.* **126** (13), 134114 (2007).
35. C. F. Craig, W. R. Duncan and O. V. Prezhdo, *Phys. Rev. Lett.* **95** (16), 163001 (2005).
36. L. Yu, C. Xu, Y. B. Lei, C. Y. Zhu and Z. Y. Wen, *Phys. Chem. Chem. Phys.* **16** (47), 25883-25895 (2014).
37. S. Mai, P. Marquetand and L. González, *WIREs Comput Mol Sci* **0** (0), DOI:10.1002/wcms.1370 (2018).
38. G. Stock and M. Thoss, *Adv. Chem. Phys.* **131**, 243-375 (2005).
39. H. T. Chen and D. R. Reichman, *J. Chem. Phys.* **144** (9), 094104 (2016).
40. U. Müller and G. Stock, *J. Chem. Phys.* **107** (16), 6230-6245 (1997).
41. I. Tavernelli, E. Tapavicza and U. Rothlisberger, *J. Mol. Struct.* **914** (1-3), 22-29 (2009).
42. T. J. Martínez, M. BenNun and R. D. Levine, *J Phys Chem-US* **100** (19), 7884-7895 (1996).
43. M. Ben-Nun and T. J. Martínez, *Adv. Chem. Phys.* **121**, 439-512 (2002).
44. G. A. Worth and I. Burghardt, *Chem. Phys. Lett.* **368** (3-4), 502-508 (2003).
45. G. A. Worth, M. A. Robb and I. Burghardt, *Faraday Discuss.* **127**, 307-323 (2004).
46. G. A. Worth, M. A. Robb and B. Lasorne, *Mol. Phys.* **106** (16-18), 2077-2091 (2008).
47. G. W. Richings, I. Polyak, K. E. Spinlove, G. A. Worth, I. Burghardt and B. Lasorne, *Int Rev Phys Chem* **34** (2), 269-308 (2015).
48. D. V. Shalashilin, *J. Chem. Phys.* **130** (24), 244101 (2009).
49. S. Romer and I. Burghardt, *Mol. Phys.* **111** (22-23), 3618-3624 (2013).
50. C. Symonds, J. A. Kattirtzi and D. V. Shalashilin, *J. Chem. Phys.* **148** (18), 184113 (2018).
51. C. Y. Zhu, A. W. Jasper and D. G. Truhlar, *J. Chem. Phys.* **120** (12), 5543-5557 (2004).
52. E. Rabani, S. A. Egorov and B. J. Berne, *J. Phys. Chem. A* **103** (47), 9539-9544 (1999).
53. Y. Z. Gan, L. Yue, X. G. Guo, C. Y. Zhu and Z. X. Cao, *Phys. Chem. Chem. Phys.* **19** (19), 12094-12106 (2017).
54. T. E. Li, A. Nitzan, M. Sukharev, T. Martínez, H. T. Chen and J. E. Subotnik, *Phys. Rev. A* **97** (3), 032105 (2018).
55. A. Jain and J. E. Subotnik, *J. Phys. Chem. A* **122** (1), 16-27 (2018).
56. N. Bellonzi, A. Jain and J. E. Subotnik, *J. Chem. Phys.* **144** (15), 154110 (2016).
57. S. C. Cheng, C. Y. Zhu, K. K. Liang, S. H. Lin and D. G. Truhlar, *J. Chem. Phys.* **129** (2), 024112 (2008).
58. M. Persico and G. Granucci, *Theor. Chem. Acc.* **133** (9), 1526 (2014).
59. E. Fabiano, T. W. Keal and W. Thiel, *Chem. Phys.* **349** (1-3), 334-347 (2008).
60. U. Werner, R. Mitric, T. Suzuki and V. Bonacic-Koutecky, *Chem. Phys.* **349** (1-3), 319-324 (2008).

61. G. Granucci, M. Persico and A. Toniolo, *J. Chem. Phys.* **114** (24), 10608-10615 (2001).
62. L. K. Du and Z. G. Lan, *J. Chem. Theory Comput.* **11** (4), 1360-1374 (2015).
63. L. K. Du and Z. G. Lan, *J. Chem. Theory Comput.* **11** (9), 4522-4523 (2015).
64. G. Granucci, M. Persico and A. Zocante, *J. Chem. Phys.* **133** (13), 134111 (2010).
65. H. D. Meyer and W. H. Miller, *J. Chem. Phys.* **70** (7), 3214-3223 (1979).
66. G. Stock and M. Thoss, *Phys. Rev. Lett.* **78** (4), 578-581 (1997).
67. H. D. Meyer and W. H. Miller, *J. Chem. Phys.* **71** (5), 2156-2169 (1979).
68. B. Li and W. H. Miller, *J. Chem. Phys.* **137** (15), 154107 (2012).
69. S. J. Cotton and W. H. Miller, *J. Phys. Chem. A* **119** (50), 12138-12145 (2015).
70. J. Liu, *J. Chem. Phys.* **145** (20), 204105 (2016).
71. J. Liu, *J. Chem. Phys.* **146** (2), 024110 (2017).
72. B. Li, E. Y. Wilner, M. Thoss, E. Rabani and W. H. Miller, *J. Chem. Phys.* **140** (10), 104110 (2014).
73. X. Sun and W. H. Miller, *J. Chem. Phys.* **106** (15), 6346-6353 (1997).
74. M. Thoss and G. Stock, *Phys. Rev. A* **59** (1), 64-79 (1999).
75. W. H. Miller, *J. Phys. Chem. A* **105** (13), 2942-2955 (2001).
76. D. V. Shalashilin and M. S. Child, *J. Chem. Phys.* **121** (8), 3563-3568 (2004).
77. M. Spanner, V. S. Batista and P. Brumer, *J. Chem. Phys.* **122** (8), 084111 (2005).
78. R. Saha and M. Ovchinnikov, *J. Chem. Phys.* **124** (20), 204112 (2006).
79. C. Venkataraman, *J. Chem. Phys.* **135** (20), 204503 (2011).
80. G. Tao, *J. Phys. Chem. A* **117** (28), 5821-5825 (2013).
81. T. J. H. Hele and N. Ananth, *Faraday Discuss.* **195**, 269-289 (2016).
82. H. H. Teh and Y. C. Cheng, *J. Chem. Phys.* **146** (14), 144105 (2017).
83. M. S. Church, T. J. H. Hele, G. S. Ezra and N. Ananth, *J. Chem. Phys.* **148** (10), 102326 (2018).
84. M. Thoss and H. Wang, *Annu. Rev. Phys. Chem.* **55** (1), 299-332 (2004).
85. H. Kim, A. Nassimi and R. Kapral, *J. Chem. Phys.* **129** (8), 084102 (2008).
86. A. Kelly and Y. M. Rhee, *J. Phys. Chem. Lett.* **2** (7), 808-812 (2011).
87. C. Y. Hsieh and R. Kapral, *J. Chem. Phys.* **138** (13), 134110 (2013).
88. H. W. Kim and Y. M. Rhee, *J. Chem. Phys.* **140** (18), 184106 (2014).
89. H. Freedman and G. Hanna, *Chem. Phys.* **477**, 74-87 (2016).
90. F. Martínez and G. Hanna, *J. Phys. Chem. A* **120** (19), 3196-3205 (2016).
91. S. Bonella and D. F. Coker, *Chem. Phys.* **268** (1-3), 189-200 (2001).
92. S. Bonella and D. F. Coker, *J. Chem. Phys.* **114** (18), 7778-7789 (2001).
93. Q. Shi and E. Geva, *J. Phys. Chem. A* **108** (29), 6109-6116 (2004).
94. P. F. Huo and D. F. Coker, *J. Chem. Phys.* **137** (22), 22a535 (2012).
95. P. Huo, T. F. M. III and D. F. Coker, *J. Chem. Phys.* **139** (15), 151103 (2013).
96. J. Provazza, F. Segatta, M. Garavelli and D. F. Coker, *J. Chem. Theory Comput.* **14** (2), 856-866 (2018).
97. N. Ananth and T. F. Miller, *J. Chem. Phys.* **133** (23), 234103 (2010).
98. G. Tao, *J. Chem. Phys.* **144** (9), 094108 (2016).
99. G. Tao, *J. Chem. Phys.* **147** (4), 044107 (2017).

100. G. H. Tao, *J. Phys. Chem. Lett.* **7** (21), 4335-4339 (2016).
101. G. H. Tao and N. Shen, *J. Phys. Chem. A* **121** (8), 1735-1748 (2017).
102. J.-L. Liao and G. A. Voth, *J. Phys. Chem. B* **106** (33), 8449-8455 (2002).
103. N. Ananth, *J. Chem. Phys.* **139** (12), 124102 (2013).
104. S. Habershon, D. E. Manolopoulos, T. E. Markland and T. F. Miller, *Annu. Rev. Phys. Chem.* **64**, 387-413 (2013).
105. S. Pierre, J. R. Duke, T. J. H. Hele and N. Ananth, *J. Chem. Phys.* **147** (23), 234103 (2017).
106. S. N. Chowdhury and P. Huo, *J. Chem. Phys.* **147** (21), 214109 (2017).
107. J. O. Richardson, P. Meyer, M. O. Pleinert and M. Thoss, *Chem. Phys.* **482**, 124-134 (2017).
108. A. E. Orel and W. H. Miller, *J. Chem. Phys.* **73** (1), 241-246 (1980).
109. R. Currier and M. F. Herman, *J. Chem. Phys.* **82** (10), 4509-4516 (1985).
110. I. Benjamin and K. R. Wilson, *J. Chem. Phys.* **90** (8), 4176-4197 (1989).
111. H. Guo and G. C. Schatz, *J. Chem. Phys.* **92** (3), 1634-1642 (1990).
112. S. Dilthey, B. Mehlig and G. Stock, *J. Chem. Phys.* **116** (1), 69-78 (2002).
113. B. Balzer, S. Dilthey, S. Hahn, M. Thoss and G. Stock, *J. Chem. Phys.* **119** (8), 4204-4215 (2003).
114. A. Ishizaki, *Chemistry Letters* **42** (11), 1406-1408 (2013).
115. W. H. Miller, W. L. Hase and C. L. Darling, *J. Chem. Phys.* **91** (5), 2863-2868 (1989).
116. G. H. Peslherbe and W. L. Hase, *J. Chem. Phys.* **100** (2), 1179-1189 (1994).
117. U. Müller and G. Stock, *J. Chem. Phys.* **111** (1), 77-88 (1999).
118. G. Stock and U. Müller, *J. Chem. Phys.* **111** (1), 65-76 (1999).
119. A. A. Golosov and D. R. Reichman, *J. Chem. Phys.* **114** (3), 1065-1074 (2001).
120. J. M. Bowman and S. C. Leasure, *J. Chem. Phys.* **66** (4), 1756-1757 (1977).
121. K. S. Bradley and G. C. Schatz, *J Phys Chem-Us* **98** (14), 3788-3795 (1994).
122. L. Bonnet and J. C. Rayez, *Chem. Phys. Lett.* **277** (1-3), 183-190 (1997).
123. G. Czako and J. M. Bowman, *J. Chem. Phys.* **131** (24), 244302 (2009).
124. A. E. Orel, D. P. Ali and W. H. Miller, *Chem. Phys. Lett.* **79** (1), 137-141 (1981).
125. S. J. Cotton and W. H. Miller, *J. Phys. Chem. A* **117** (32), 7190-7194 (2013).
126. S. J. Cotton, K. Igumenshchev and W. H. Miller, *J. Chem. Phys.* **141** (8), 084104 (2014).
127. W. H. Miller and S. J. Cotton, *Faraday Discuss.* **195**, 9-30 (2016).
128. W. H. Miller, *J. Chem. Phys.* **61** (5), 1823-1834 (1974).
129. W. H. Miller and S. J. Cotton, *J. Chem. Phys.* **142** (13), 131103 (2015).
130. S. J. Cotton, R. B. Liang and W. H. Miller, *J. Chem. Phys.* **147** (6), 064112 (2017).
131. A. A. Kananenka, C.-Y. Hsieh, J. Cao and E. Geva, *J. Phys. Chem. Lett.*, 319-326 (2017).
132. S. J. Cotton and W. H. Miller, *J. Chem. Phys.* **145** (14), 144108 (2016).
133. J. Zheng, Y. Xie, S. s. Jiang, Y. z. Long, X. Ning and Z. g. Lan, *Chin. J. Chem. Phys.* **30** (6), 800-810 (2017).

134. S. J. Cotton and W. H. Miller, *J. Chem. Theory Comput.* **12** (3), 983-991 (2016).
135. G. Tao, *J. Chem. Theory Comput.* **11** (1), 28-36 (2015).
136. S. J. Cotton and W. H. Miller, *J. Chem. Phys.* **139** (23), 234112 (2013).
137. G. Tao, *J. Phys. Chem. C* **118** (31), 17299-17305 (2014).
138. G. Tao, *J. Phys. Chem. C* **118** (47), 27258-27264 (2014).
139. A. Kelly, R. van Zon, J. Schofield and R. Kapral, *J. Chem. Phys.* **136** (8), 084101 (2012).
140. S. Bonella and D. F. Coker, *J. Chem. Phys.* **122** (19), 194102 (2005).
141. Q. Shi and E. Geva, *J. Chem. Phys.* **120** (22), 10647-10658 (2004).
142. W. H. Miller and S. J. Cotton, *J. Chem. Phys.* **145** (8), 081102 (2016).
143. G. H. Tao, *J. Phys. Chem. C* **120** (13), 6938-6952 (2016).
144. S. Jiang, J. Zheng, Y. Yi, Y. Xie, F. Yuan and Z. Lan, *J. Phys. Chem. C* **121** (49), 27263-27273 (2017).
145. Y. Xie, J. Zheng and Z. Lan, *J. Chem. Phys.* **142** (8), 084706 (2015).
146. H. Tamura, I. Burghardt and M. Tsukada, *J. Phys. Chem. C* **115** (20), 10205-10210 (2011).
147. Q. Meng, S. Faraji, O. Vendrell and H.-D. Meyer, *J. Chem. Phys.* **137** (13), 134302 (2012).
148. J. Zheng, Y. Xie, S. Jiang and Z. Lan, *J. Phys. Chem. C* **120** (3), 1375-1389 (2016).
149. O. Vendrell and H.-D. Meyer., in *O. Vendrell and H.-D. Meyer, Version 8.5 (2011)*. See <http://mctdh.uni-hd.de>.
150. A. Ishizaki and G. R. Fleming, *J. Chem. Phys.* **130** (23), 234111 (2009).
151. H. Ma and A. Troisi, *Adv. Mater.*, 6163–6167 (2014).
152. Y. Yao, X. Xie and H. Ma, *J. Phys. Chem. Lett.* **7** (23), 4830-4835 (2016).
153. M. Thoss, H. B. Wang and W. H. Miller, *J. Chem. Phys.* **115** (7), 2991-3005 (2001).
154. E. Thiele, *J. Chem. Phys.* **39** (12), 3258-3262 (1963).
155. G. Z. Whitten and B. S. Rabinovitch, *J. Chem. Phys.* **38** (10), 2466-2473 (1963).
156. M. Berblinger and C. Schlier, *J. Chem. Phys.* **96** (9), 6834-6841 (1992).
157. M. Buchholz, E. Fallacara, F. Gottwald, M. Ceotto, F. Grossmann and S. D. Ivanov, *Chem. Phys.*, DOI: 10.1016/j.chemphys.2018.1006.1008 (2018).